Int. J. Electrochem. Sci., 14 **(2019)** 5200 – 5210, doi: 10.20964/2019.06.05

International Journal of ELECTROCHEMICAL SCIENCE
www.electrochemsci.org

Fabrication and Characterization of Polypyrrole/Reduced Graphene-Oxide Films for Electrochemical Capacitors

O. J. Márquez-Calles[1]*, R. D. Martínez-Orozco*[1]*, N. V. Gallardo-Rivas*[1]*, A. M. Mendoza-Martínez*[1]*, R. Mayén-Mondragón*[2] *and U. Páramo-García*[1*]

[1] Tecnológico Nacional de México/Instituto Tecnológico de Cd. Madero, Centro de Investigación en Petroquímica, Prol. Bahía de Aldhair y Av. de las Bahías, Parque de la Pequeña y Mediana Industria, 89600, Altamira, Tamaulipas, México.
[2] Polo Universitario de Tecnología Avanzada, Facultad de Química, Universidad Nacional Autónoma de México, 66629, Apodaca, Nuevo León, México
[*]E-mail: uparamo@itcm.edu.mx

Received: 13 November 2018 / *Accepted:* 23 March 2019 / *Published:* 10 May 2019

The co-electrodeposition and characterization of Polypyrrole (PPy)/Reduced Graphene Oxide (RGO) films (1:5, 1:10 and 1:15 mass ratio) for electrochemical capacitors are presented in this work. Polypyrrole polymerization and incorporation of RGO were conducted simultaneously in order to attain the best possible dispersion of the latter within the polypyrrole matrix. The materials were characterized by scanning electron microscopy, Fourier-transform infrared spectroscopy, X-ray diffraction and electrochemical impedance spectroscopy (EIS). The effect of the RGO:PPy mass ratio on the film electrochemical and morphological properties was evaluated. The results show a good dispersion of RGO was attained, along with a good cycling stability of the composite materials. Agglomeration of the PPy was however observed. EIS analysis showed the composite capacitance increases as the RGO content is increased. The polarization resistance, on the other side, increased unexpectedly for larger PPy contents due mainly to agglomeration effects and over-oxidation of the conductive polymer. A finer dispersion of the PPy phase is imperative to improve the electrochemical properties of the composite.

Keywords: RGO:PPy, composite materials, capacitors, thin films, electrodeposition.

1. INTRODUCTION

In recent years, the use of energy storage devices such as electrochemical capacitors have increased considerably. Efforts are thus being directed towards the implementation of more efficient, economic and of course, environmentally-friendly methods for their manufacture. The selection of electrode materials is critical since it impacts the device electrochemical performance, and in this sense, may lead to improvements in the overall capacitance. Conductive polymers can be implemented as supercapacitor electrode materials due to their good electrical conductivity, high charge density, low cost and excellent pseudocapacitor behavior [1]. They can be synthesized by electrochemical methods which themselves allow a fine control of processing variables such as pH, oxidation potential, temperature, type of dopant anion, among others. They are as well environmental-friendly since the main reagent is the electron [1-5].

Polymer-based capacitors, such as those based on Polypyrrole (PPy), Polyaniline (PANi) and Polytiophene (PTh), as well as those incorporating activated carbon, carbon nanotubes and graphene have recently attracted considerable attention. Many researchers have tested combinations of those materials to benefit from the pseudocapacitance of conductive polymers and the large capacitance of the carbonaceous-materials double-layer [1, 2, 6-10]. The high surface area normally present in carbon-based electroactive materials facilitates the transport of ionic species during the charge-discharge process. At the same time, it allows for a better dispersion during the preparation of the composite materials. Graphene has become one of the favorite materials due to its huge theoretical surface area, high mobility of charge carriers, high electrical conductivity, large mechanical strength and high thermal conductivity [1, 6]. PPy has also been extensively implemented due to its high electrical conductivity and good stability when exposed to environmental conditions, as well as its fine capacitive properties.

The electrochemical aspects related to the synthesis of PPy and carbon-based electroactive materials are a great research opportunity [11, 12]. Even when electrodeposition is an effective method for preparing films based on PPy/Reduced Graphene Oxide (RGO) composites, the reported synthesis conditions are still broad in range. Some authors have even included metallic nanoparticles into the formula looking to improve the composite stability. Eeu *et al.* incorporated Fe_2O_3 to form a ternary material [13]. Their nanocomposite stability was positively influenced, however an increase in the charge transfer resistance was observed [13]. The combination of carbon-based materials and conductive polymers is an alternative way to improve stability. It enhances as well capacitance and thus the performance of a supercapacitor. Such composites have resulted in high electrical conductivity essential to their application as supercapacitor electrodes [14-17]. By adjusting the mass ratio of RGO and PPy during the electropolymerization process, important variations of the composite properties can be achieved. Otherwise, the structure and morphology of the composite materials can be modified according to the selected synthesis parameters.

In this study we present the co-electrodeposition and physicochemical characterization of conductive polymer films with different PPy and RGO mass ratios. The films were electrosynthesized by cyclic voltammetry on a stainless steel substrate, applying different inversion potentials, the latter being related to the oxidation level of the Pyrrole monomer (Py).

2. EXPERIMENTAL

The synthesis of Graphene Oxide (GO) was carried out by the Hummer´s method [18], which involves steps of graphite oxidation/exfoliation in an acid medium. Graphite powder, sulfuric acid and potassium permanganate of analytical degree were used. PPy/RGO films were fabricated by cyclic voltammetry (CV) at a potential scan rate of 100 mV/s using a potentiostat/galvanostat Autolab model 302N, and a conventional three-electrode cell. Stainless steel plates were used as working (WE) and auxiliary electrodes. The plates were first mechanically polished and afterwards immersed in an ultrasound distilled-water bath for 10-15 minutes (BAKU ultrasound system, 3550). A Platinum wire was in some experiments used as an auxiliary electrode. An Ag/AgCl (BAS, MF-2052) electrode was used as reference and protected from the experimental medium by a porous Vycor membrane. A 0.1 M KCl solution (Fermont, ACS) served as electrolyte. The experiments were performed at room temperature. The sample solutions were prepared with distilled water (Fermont) and deionized water (Analytyka). The PPy/RGO solution consisted of 0.1 g GO and 10 ml deionized water. The solution was ultrasound-mixed during 30 min, and then the Py monomer (Py, Aldrich, 98%) was added. The solution was then set to 40 cycles of polymerization by cyclic voltammetry, in the aqueous KCl electrolyte.

The electrochemical behavior of the fabricated materials was studied by electrochemical impedance spectroscopy. A sinusoidal potential signal of 15 mV amplitude was applied in the frequency range of 1 MHz to 10 mHz [19]. Complex (Nyquist) plots were fitted to four-element equivalent-electric-circuits to determine the polarization resistance and double layer capacitance.

The morphological characteristics of the materials were analyzed by scanning electron microscopy (SEM) using an XL30 ESEM Philips microscope operated at 2 kV. Attenuated-total-reflection Fourier-transform IR (ATR-FTIR, Spectrum GX, Perkin Elmer) spectroscopy was employed to determine the chemical composition. Bulk X-ray diffraction (RIGAKU Dmax 2100 diffractometer) and Raman spectra (Brama HR Evolution HORIBA Scientific, with red and green wavelength lines) were used to check composition and crystal structure.

3. RESULTS AND DISCUSSION

Figure 1 shows the 1st, 10th, 20th, 30th and 40th polymerization cycle of PPy-RGO (1:5 mass ratio) under 0.9 V (Fig 1a) and 0.95 V (Fig. 1b) inversion potentials. The characteristic pattern of an irreversible oxidation process can be readily identified. Such response may be attributed to the Py monomer oxidation. The different redox processes occurring during the PPy polymerization can not be resolved due to the presence of RGO. For the 0.95 V overpotential (Fig. 1b), over-oxidation of the PPy film modifies the curve morphology. This affects the material properties and, particularly, its stability and adhesion. [3-5]

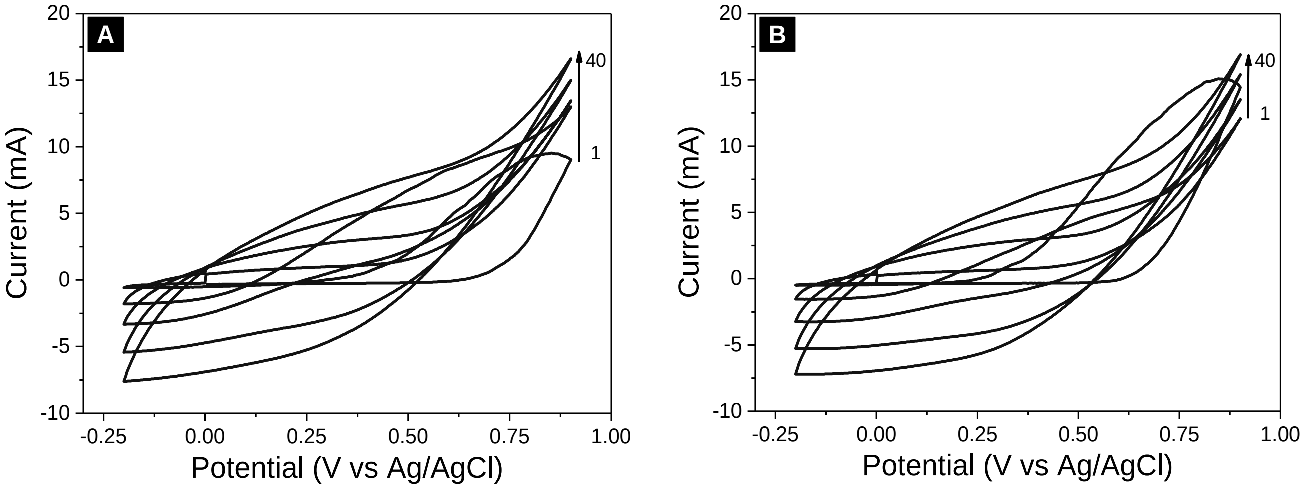

Figure 1. Cyclic voltammograms of RGO:PPy films electrodeposited at a mass ratio of 1:5 for an inversion potential vs Ag/AgCl of A) 0.90 V and B) 0.95 V (cycles 1st, 10th, 20th, 30th and 40th).

Figure 2 shows the 40th polymerization cycle for the electrodeposited films, under a potential window of -0.2 to 0.95 V, and with different GO:PPy mass ratios (0:1 or without GO, 1:5, 1:10 and 1:15). The area enclosed by the curve represents the amount of electrodeposited material. It can be observed that as the GO content becomes more significative, such area undergoes changes, a characteristic related to the intercalation capacity of the fabricated materials.

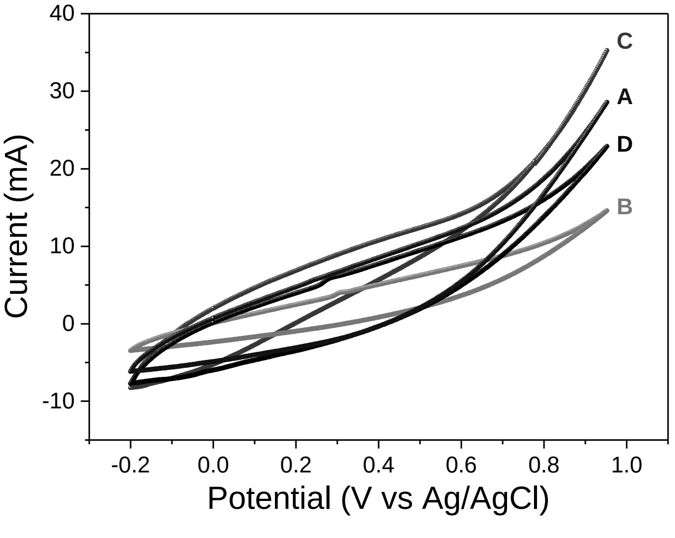

Figure 2. Cyclic voltammogram (40th cycle) of the electrodeposited films prepared with different RGO:PPy mass ratio: a) 0: 1, b) 1: 5, c) 1:10 and d) 1:15 respectively.

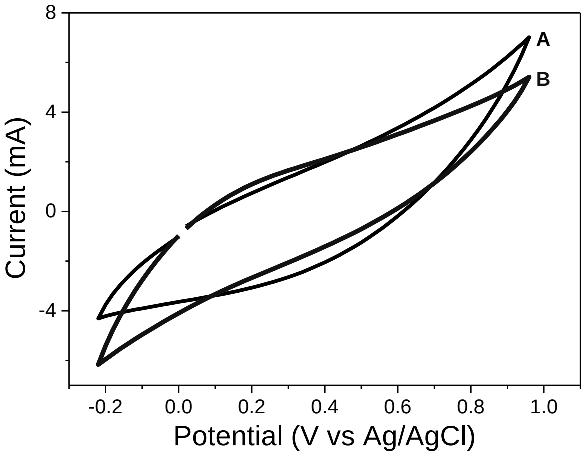

Figure 3. Stability test of a 1:15 RGO:PPy electrodeposited film. Charge/discharge cycles at 200 mV/s, a) 1st cycle and b) 200th cycle.

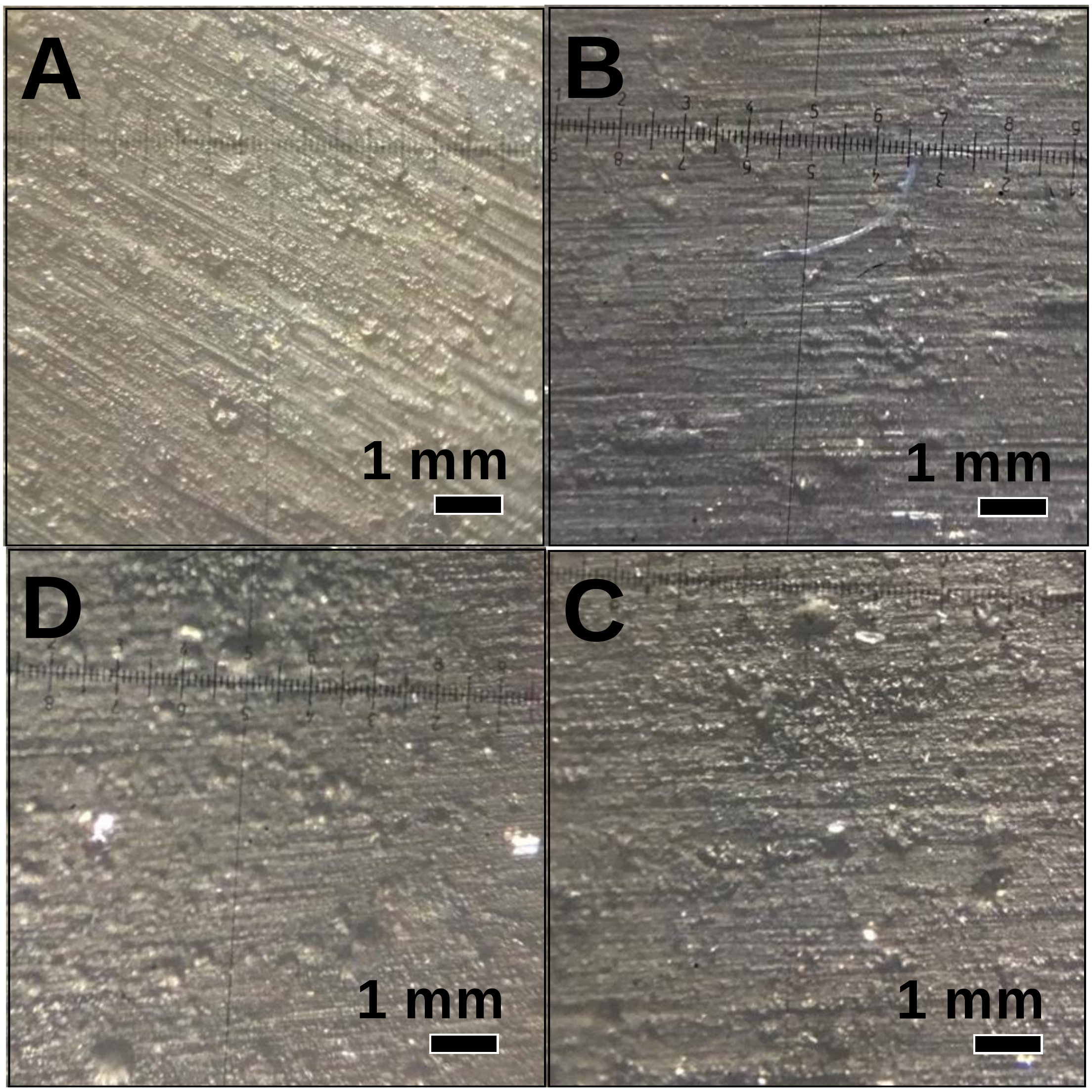

Figure 4. Optical microscopy micrographs of the RGO:PPy films with mass ratio of: a) 0:1, b) 1:5, c) 1:10 and D) 1:15 respectively.

The cycling stability of the prepared materials was investigated applying 200 cyclic-voltammetry scans from -0.2 to 0.95 V, at 200 mV/s, in an aqueous solution of 0.1 M KCl. Figure 3 shows the first and the last cycle for the 1:15 GO: PPy mass ratio. The area enclosed by the curve was only slightly decreased between the first and last cycle. This points to a good stability of the material, and thus, to its possible application for capacitor electrodes. [20]

Figure 4 shows optical-microscopy micrographs of the RGO:PPy films after the stability tests. The films were observed to grow in a non-uniformly fashion (polymerization starts up on certain localized regions and grows there on, resulting in lower-adhesion spots). Shiny spots on the micrographs correspond to regions with an exposed stainless steel surface. The latter is attributed to material degradation or detachment during the charge/discharge tests.

Figure 5 shows scanning-electron-microscopy micrographs of the RGO:PPy films. The characteristic morphology of PPy materials electrodeposited by cyclic voltammetry can be observed in Figure 5a. It is observed quasi-amorphous with 3D structure and cauliflower-type aggregates. [3, 5] Incorporation of RGO during the co-electrodeposition process modifies the surface morphology. The PPy features become reorganized and the material tends to form thick layers (Figures 5b, 5c and 5d). The composite agglomeration level must be minimized. Incorporation of RGO has to be then performed in a controlled manner to attain a good dispersion. This should allow maximizing the pseudocapacitance and electrical double-layer capacitance. At the same time, the diffusion and migration pathways of electrolyte ions should be reduced, allowing faster electrochemical charge/discharge cycles. [21, 22]

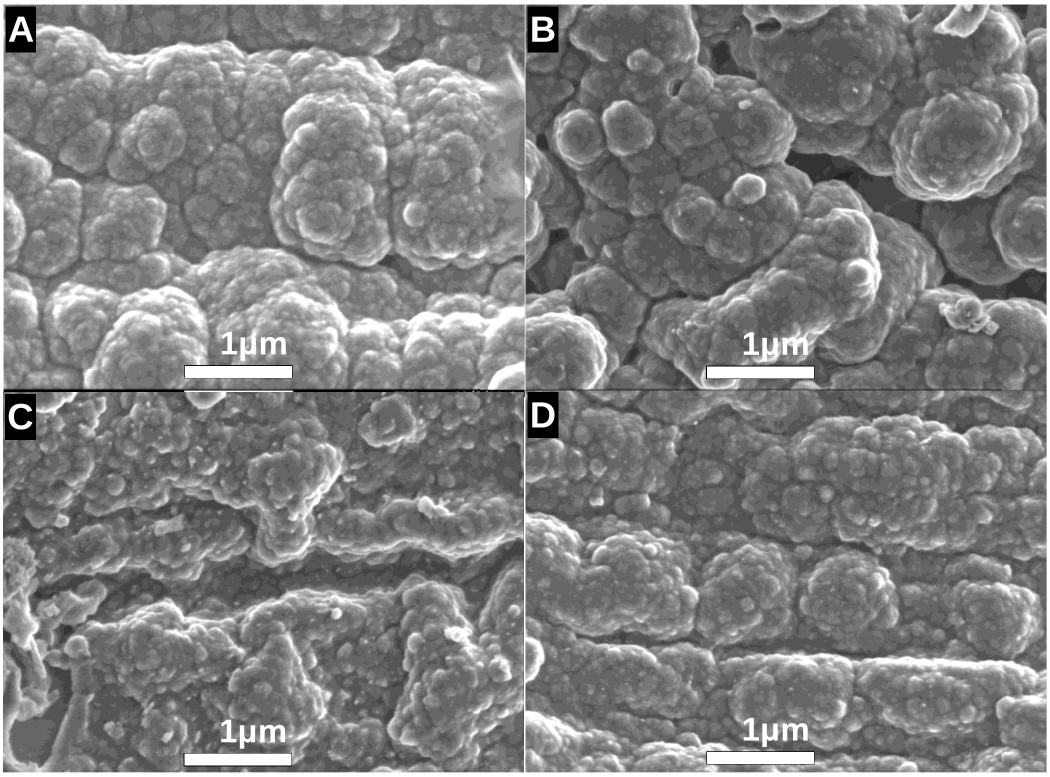

Figure 5. SEM micrograpsh of the films with different RGO:PPy mass ratio: a) 0: 1, b) 1: 5, c) 1:10 and d) 1:15.

Figure 6 shows the ATR-FTIR spectra of the RGO/PPy fabricated films. No RGO-attributed vibration bands were observed. Either the characteristic functional groups were eliminated or masked. The peaks at 1550 cm^{-1} and 1460 cm^{-1} are characteristic of the symmetric stretching vibrations of C-C, C-N and N-H, respectively, in the PPy rings (Fig. 6A). While the bands at 1300 cm^{-1} and 1030 cm^{-1} are due to the C-N stretching and C-H bond vibration of the PPy plane, respectively. The band at 910 cm^{-1} is attributed to the flexural vibration outside the C-C plane, suggesting good pyrrole polymerization. [21, 23] For systems with different GO ratios, the peaks assigned to the PPy can still be observed, however shifted to higher wavelengths, depending on the GO-amount added (Fig. 6B, 6C and 6D). This fact confirms the reduced graphene oxide was succesfully introduced into the PPy matrix, validating thus the co-electrodeposition process.

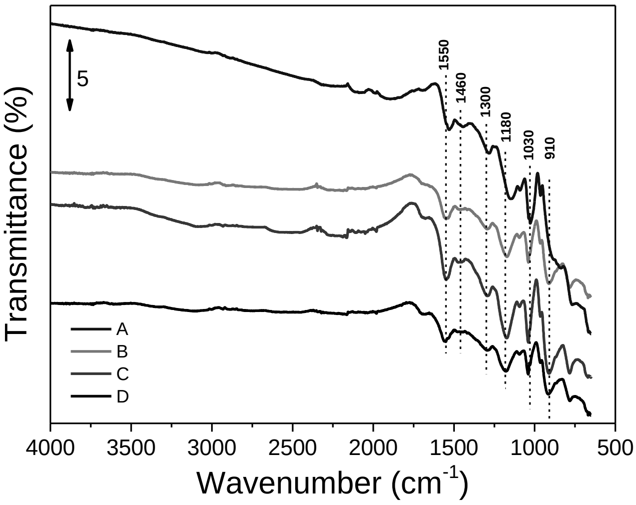

Figure 6. ATR-FTIR spectra of the films with different RGO:PPy mass ratio: A) 0: 1, B) 1: 5, C) 1:10 and D) 1:15.

Figure 7 shows the Raman spectra of the fabricated films. The results provide structural information of carbon composite materials. The characteristic spectrum of the PPy can be observed in figure 7A. It includes two broad bands at 1330 and 1559 cm^{-1} due to stretching of C-C and the stretching mode of the ring, respectively. [21,23] Other characteristic peaks are observed at 620, 676, 950, 1075 and 1250 cm^{-1} attributed to the ring torsion, movement of the CH bond, deformation of the ring associated with the direction, symmetrical flexion of the C-H plane and the N-H deformation in the plane, as well as the C-H bending in the antisymmetric plane, respectively. In the case of the GO signals (Fig. 7B), two characteristic peaks are observed at 1310 cm^{-1} and 1600 cm^{-1} corresponding to the D and G bands. The D band is associated with the optical vibration in the plane, whereas the G band is due to the first order zone of the phonons. The RGO: PPy samples spectrum show as well the D and G band signals at 1311 and 1659 cm^{-1}, however the intensity of the D/G ratio increases in comparison with the graphene oxide signal by itself (RGO).

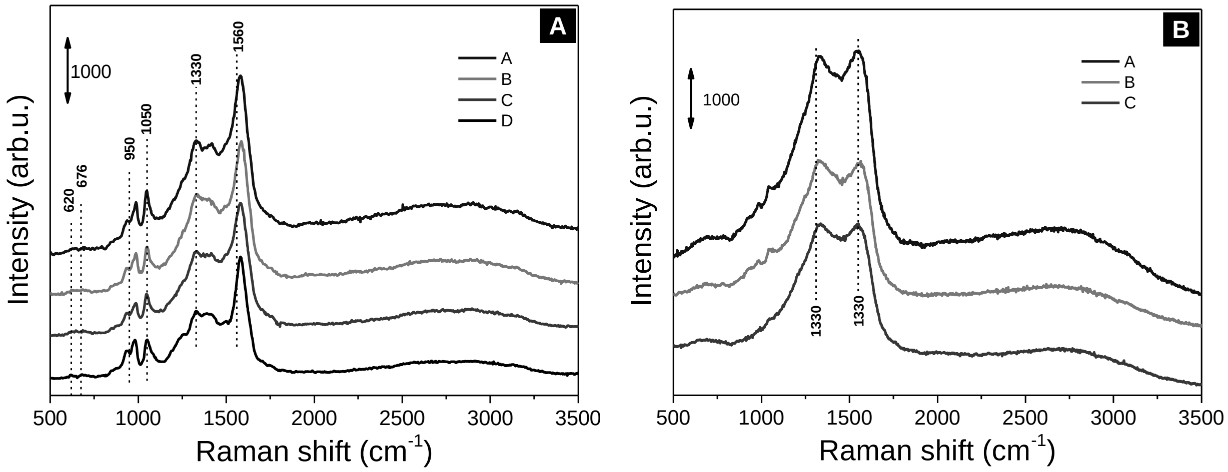

Figure 7. Raman spectra of the electrodeposited RGO:PPy films with different mass ratio: A) 0: 1, B) 1: 5, C) 1:10 and D) 1:15. Laser: a) green and b) red.

Figure 8 shows the x-ray diffraction patterns (XRD) of the PPy and composite films with different RGO: PPy mass ratio.

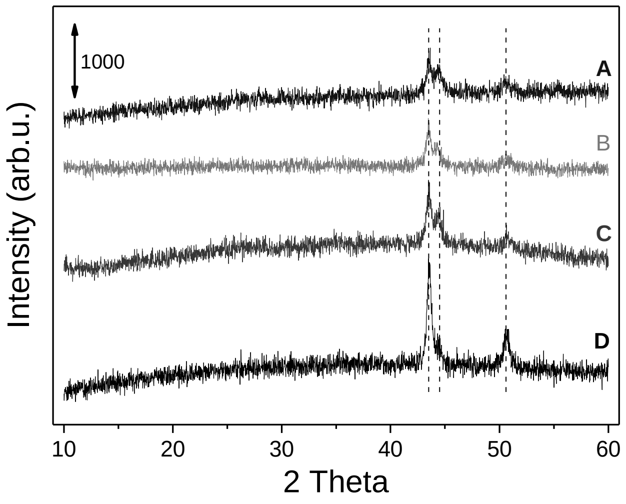

Figure 8. X-ray diffraction patterns of the RGO:PPy films with different mass ratio: A) 0: 1, B) 1: 5, C) 1:10 and D) 1:15. NOTE: The results only show the signals of the substrate.

Natural graphite shows high-intensity diffraction peaks at 2θ = 26.3° and 54.5° [7]. GO, on the other side, reveals a characteristic peak (001 plane) around 2θ = 11.7° corresponding to an interlayer spacing of 0.80 nm. It results from the electrochemical oxidation at the potential of 0.95 V vs Ag/AgCl, which interrupts the graphene layers ordering, and introduces functional groups such as epoxy, hydroxyl (OH), carboxyl (COOH) and carbonyl (C = O) at the edges and both sides of the graphene sheets. The pristine PPy form exhibits a wide diffraction peak around 2θ = 25°, which basically indicates an amorphous nature, corroborating the SEM micrographs observations (Fig. 5). Due to the amorphous PPy features and the thickness of the electrodeposited films, all the XRD diffractograms in Fig. 8 present signals which correspond to the stainless steel substrate.

Figure 9 shows the Nyquist plots of the electrodeposited RGO: PPy films with three different mass ratios, 1:5, 1:10, 1:15. Capacitive semicircles can be observed within the mid frequency range. The semicircles are related to the electric double layer capacitance and the main charge transfer process at the electrode surface. At lower frequencies, a distinctive tail can be observed. It is attributed to mass transfer by semi-infinite diffusion. Figure 10 shows the equivalent circuit fit to the Nyquist plots, while Table 1 presents the circuit-element values obtained from the fitting procedure. Rs corresponds to the solution resistance (Ohm), Rp is the charge transfer resistance (Ohm), CPE is the constant phase element characterized by the exponent n (dimensionless) and Q_0 (Ohm^{-1} s^{n}), and W is the Warburg impedance (Ohm s$^{-0.5}$). An increase in the CPE coefficient Q_0 can be observed as the PPy content of the material is reduced. This may be an indicator of the reduced-graphene-oxide main contribution to the overall composite capacitance. The RGO, however, shows a more marked capacitance dispersion (the dimensionless exponent n decreases as the PPy content is reduced). The "true" capacitance calculated from the capacitive-semicircle-elements is 0.044 Farad for the 1:5 composite. Several values of specific capacitance for RGO:PPY composites can be found in the literature [7,8,9,10]. However, we could not directly perform a comparison as we do not know at the moment the exact weight of composite deposited onto the electrodes. Future experiments however will include deposition using a Quartz Crystal Microbalance to that end.

Regarding the Warburg parameter σ, a tendency to decrease when reducing the PPY content was observed. Such effect is understandable considering how the well-dispersed RGO should facilitate the transport of ionic species during the charge-discharge process. It is noteworthy mentioning that, on the other side, the increase in PPy concentration did not show the expected reduction in charge transfer resistance. We believe this to result from the inconvenient agglomeration of the PPy phase, reducing mainly the active surface-area, as well as from over-oxidation of the conductive polymer. A finer dispersion of the material should be sought in order to improve the electrochemical-capacitor behavior of the electrode.

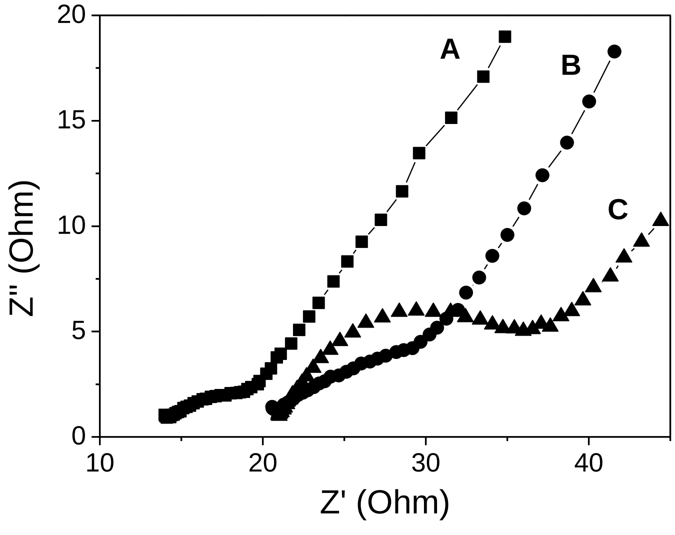

Figure 9. Nyquist plots of the electrodeposited RGO:PPy films with three different mass ratios: A) 1: 5, B) 1:10, C) 1:15.

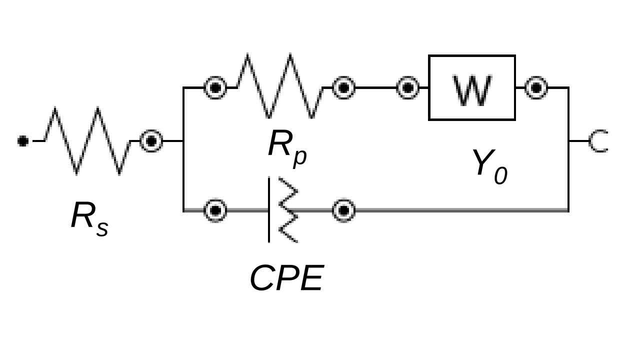

Figure 10. Equivalent circuit fit to the Nyquist plots of the RGO:PPy films with mass ratio 1: 5, 1:10, and 1:15.

Table 1. Circuit-element values obtained by fitting the Nyquist plots in Figure 9 to the equivalent circuit shown in Figure 10.

	Rs	R	13	Ohm
	Rp	R	7	Ohm
	CPE	Q_0	8E-2	Siemens*s^n
		n	0.5	
	W	σ	1.35	Ohm*s^-0.5
	Rs	R	20	Ohm
	Rp	R	10	Ohm
	CPE	Q_0	7E-2	Siemens*s^n
		n	0.65	
	W	σ	1.65	Ohm* s^-0.5
	Rs	R	21	Ohm
	Rp	R	14	Ohm
	CPE	Q_0	3E-2	Siemens*s^n
		n	0.85	
	W	σ	1.44	Ohm*s^-0.5

4. CONCLUSIONS

Successful co-electrodeposition of Polipirrole (PPy) / Reduced Graphene Oxide (RGO) films with 1: 5, 1:10 and 1:15 mass ratios were achieved in the present work. A good RGO dispersion within the PPy matrix was attained but agglomeration of the PPY phase was also observed. A larger amount of polymer was produced when applying the broadest potential window of -0.2 to 0.95V vs Ag/AgCl. However, PPy over-oxidation became more apparent than if the potential window was limited to 0.90 V. Good cycling stability was observed for all the fabricated composites. The capacitance of the PPY was enhanced due to the RGO incorporation. However, the composite did not show the expected polarization-resistance reduction when increasing the PPY content. We believe this to be caused by the unwanted PPY agglomeration and over-oxidation of the polymer. Nevertheless, more work has to be done in this direction to better understand the effect of processing variables over the composite electrochemical behavior. In the end, we are seeking to increase the composite chances of being successfully implemented as electrode material for electrochemical capacitors.

ACKNOWLEDGMENTS
O.J. Marquez-Calles acknowledges the scholarship provided by CONACYT-Mexico. We would like to thank Tecnológico Nacional de México (TecNM) for the reagents and materials provided through funding from the 6254.17-P project.

References

1. H. A. Hamra, H. N. Lim, S. Kamaruzaman, S. A. Rashid, R. Yunus, N. M. Huang, C. Y. Yin, M. M. Rahman, M. Altarawneh, Z. T. Jiang and P. Alagarsamy, *Nanos. Res. Lett.*, 12 (2017) 1.
2. P. Asen and S. Shahrokhian, *J. Phys. Chem*. C, 121 (2017) 6508.
3. A. Aphale, K. Maisuria, M. K. Mahapatra, A. Santiago, P. Singh and P. Patra, *Sci. Reports*, 5 (2015) 1.
4. W. S. Hummers and R. E. Offeman, *J. Am. Chem. Soc.*, 80 (1958) 1339.
5. U. Páramo-García, J. G. Ibanez and N. Batina, *Int. J. Electrochem. Sci.*, 6 (2011) 5172.
6. U. Páramo-García, N. Batina and J. G. Ibanez, *Int. J. Electrochem. Sci.*, 7 (2012) 12316.
7. C. Zhao, K. Shu, C. Wang, S. Ghambhir and G. G. Wallace, *Electrochim. Acta*, 172 (2015) 12.
8. T. Qian, C. Yu, S. Wu and J. Shen, *J. Mater. Chem. A*, 1, (2013), 6539.
9. N. Lingappan, Y.-S. Gal and K. T. Lim, *Mol. Cryst. Liq. Cryst.*, 585 (2013) 60.
10. H. D. Pham, V. H. Pham, E.-S. Oh, J. S. Chung and S. Kim, *Korean J. Chem. Eng.*, 29 (2012) 125.
11. U. Páramo-García, J. G. Ibanez and N. Batina, *Int. J. Electrochem. Sci.*, 8 (2013) 2656.
12. C. Hao-Hsiang, C. Chih-Kai, T. Yu-Chen and L. Chien-Shiun, *Carbon*, 50 (2012) 2331.
13. Y. C. Eeu, H. N. Lim, Y. S. Lim, S. A. Zakarya, and N. M. Huang, *J. Nanomat*., (2013) 1.
14. Y. Liu, H. Wang, J. Zhou, L. Bian, E. Zhu, J. Hai, J. Tang and W. Tang, *Electrochim. Acta*, 112 (2013) 44.
15. H. P. Oliveira, S. A. Sydlik and T. M. Swager, *J. Phys. Chem*. C, 117 (2013) 10270.
16. J. Chen, Y. Wang, J. Cao, Y. Liu, Y. Shou, J-H. Ouyang and D. Jia, *Appl. Mater. Interfaces*, 9 (2017) 19831.
17. N. Naidek, A. J. G. Zarbin and. E. S. Orth, *J. Pol. Sci. A: Pol. Chem*., 56 (2018) 579.
18. W. S. Hummers Jr. and R. E. Offeman, *J. Am. Chem. Soc*., 80 (1958) 1339.
19. U. P. Morales, E. V. López and C. O. Otálora, *Dyna*, 162 (2010) 13.
20. N. Sarlak and T. J. Meyer, *J. Mol. Liq*., 243 (2017) 243.
21. F. Zhang, F. Xiao, Z. H. Dong and W. Shi, *Electrochim. Acta*, 114 (2013) 125.
22. M. Li, X. Ji, L. Cui and J. Liu, *J. Mater. Sci*., 52 (2017) 12251.
23. S. F. Besharat, M. Manteghian and M. Abdollahi, *Pol. Sci*. B, 60 (2018) 664.